Retrievals of Key Biophysical Parameters at Mesoscale from the Ts/VI Scatterplot Domain

George P. Petropoulos[1,*], Dionissios Hristopulos[1]

[1] *School of Mineral Resources Engineering, Technical University of Crete, Chania, 73100, Greece*

*Correspondence to: petropoulos.george@gmail.com; gpetropoulos1@isc.tuc.gr Tel: +30 (0) 28210 37642

ABSTRACT

Earth Observation (EO) employed often in synergy with simulation process models provides a promising direction for acquiring information on key parameters required to understand the Earth's system physical mechanisms and interactions. The objective of this study is two-fold: First, it explores the combined use of EO data from the Advanced Along-Track Scanning Radiometer (AATSR) with the SimSphere land biosphere model via the "triangle" to derive latent (LE) and sensible heat (H) fluxes and soil moisture content (SMC) over diverse European ecosystems. Secondly, it investigates the influence of atmospheric correction on the "triangle"-derived retrievals. For this purpose, both non-atmospherically (AATSR 1P) and atmospherically corrected (AATSR 2P) AATSR data products are used. Those were acquired for selected days spanning from 2007 to 2011 at 12 sites belonging to a European ground monitoring network. The comparison of the predictions from the 1P product against the *in-situ* measured SMC resulted in an RMSD of 0.13 cm cm^{-1}, which improved to 0.06 cm^3 cm^{-3} when the 2P product was utilised. The correlation coefficient (R) was also satisfactory for both product levels (R=0.766 for the 1P versus R=0.844 for the 2P product). The daytime-averaged fluxes also improved by using the 2P products with RMSD values of 0.146 and 0.130 for the daytime averages of LE and H fluxes respectively. For all predicted parameters the statistical measures notably improved when the 2P product is utilised (with R of 0.92 and 0.69 for the LE and H fluxes respectively). Comparisons showed a variant agreement between the predicted parameters and the measured values depending on the land cover type. The findings are significant since to our knowledge, the present study for the first time addresses the following issues: (1) It assesses the triangle technique at a mesoscale resolution of 1 km using AATSR data, offering important information regarding the surface heterogeneity effect on the parameters retrieval accuracy. (2) It investigates the effect of atmospheric correction on the technique's prediction accuracy, thus addressing an scientific knowledge gap in its application, as such errors can lead to higher uncertainty and biases in the "triangle"-derived retrievals. These findings provide important information regarding the future utilisation of the investigated technique for potential operationalisation.

KEYWORDS: *latent heat, sensible heat, soil moisture, AATSR, triangle, SimSphere*

1. INTRODUCTION

Earth's physical mechanisms, interactions and feedback processes between its land surface and atmosphere are key elements in forming our physical environment (Seneviratne et al., 2010; Sun et al., 2019). These land-surface interactions include the numerous complex natural processes which also influence the global climate system (Stoyanova and Georgiev, 2013; North et al., 2015). Thus, understandably, accurate information about such climate parameters over a variety of space and time scales is essential to assess the dynamics and distribution of key biophysical variables and to ensure long-term stability of terrestrial ecosystem services (Bao et al., 2018). In particular, parameters such as soil moisture content (SMC), combined with sensible (H) and latent heat (LE) heat are key state variables affecting numerous Earth's processes (Vereecken et al., 2014; Shi and Liang, 2014; Deng et al., 2019a). Accurate estimation of their spatiotemporal variability is thus of prime interest for many research investigations, practical applications and in addressing key societal challenges today linked to global societal challenges such as food and water security (Petropoulos et al., 2015; Silva-Fuzzo et al., 2019).

Accurate information on the spatiotemporal variability of both LE/ H fluxes and of SMC over large scales can be very expensive and time consuming (Petropoulos & McCalmont, 2017), particularly so over highly heterogeneous areas. In this respect, Earth Observation (EO) is recognised today as a promising avenue in estimating turbulent fluxes of LE and H and/or SMC. Numerous techniques have been developed for this purpose that utilise data obtained across the range of electromagnetic spectrum, with their relevant implementation strengths and weaknesses already well-documented in the literature (see recent reviews by Petropoulos et al., 2018a,b; Petropoulos et al., 2015). A special group of EO-based methods includes those which combine the surface temperature (Ts) with a Vegetation Index (VI), where empirical relations are obtained by plotting Ts against VI, termed as Ts/VI methods (for an extensive review see Petropoulos et al., 2009a). Compared to other EO-based modelling approaches employed in the retrievals of energy fluxes and/or SMC, Ts/VI techniques are characterised by an enhanced capability to account for land surface heterogeneity. In addition to this, their implementation is based on easily obtainable from EO data which also makes them also an ideal candidate for operational implementation.

Some researchers have proposed the use the Ts/VI domain synergistically with a land surface process model in obtaining information on both LE/H fluxes and SMC from EO data, commonly termed as the "triangle" (Petropoulos et al., 2014; Carlson & Petropoulos, 2019). This approach allows merging the spectral resolution and horizontal coverage of EO data with the detailed description of the physical processes vertically and the fine prediction time step of SVAT models. One of the key is that it links the Ts/VI feature space with the predicted LE/H fluxes and SMC in a non-linear relationship, which is more realistic than the assumption of linearity provided by most other Ts/VI methods. In addition, it offers the potential for relatively easy transformation of the derived fluxes for each satellite overpass time to daytime averages. Various studies have already demonstrated the "triangle's" ability to predict LE and H fluxes and SMC with accuracy in the range between 40 and 70 Wm^{-2} and within 5 % cm^3 cm^{-3} for SMC, which is considered a satisfactory prediction for many applications (Gillies et al., 1997; Petropoulos and Carlson, 2011). A variant of the "triangle" is at present operationally implemented to map SMC over Spain at 1 km based on ESA's SMOS satellite (Piles et al., 2011). Also, modified versions of this approach have been under investigation towards the operational level development of relevant products (Chauhan et al., 2003; ESA STSE, 2012).

Yet, to our knowledge, investigation of this method accuracy on a meso- to macro-scale as well as for European ecosystems is limited. Indeed, studies that have been concerned with the validation of the "triangle" investigated primarily when that is applied with fine spatial resolution EO data, and on US ecosystems. Interestingly, most of these studies have also been concerned only with the validation of instantaneous SMC and energy flux estimates. Hence, very little is known practically on the methods' accuracy for daytime average estimates. Verification of the "triangle" at coarser spatial resolution (e.g. of 1km or higher) will offer important information on the surface heterogeneity effect on the retrieval accuracies of the target parameters. Furthermore, the "triangle" has been implemented in studies which have utilised either atmospherically or non-atmospherically corrected data. Hence, little is known at present on the atmospheric correction effect on the technique's prediction accuracy. This is an important scientific knowledge gap, as errors in satellite derived Ts and VI could lead to uncertainty and biases in the "triangle"-derived retrievals. It is known that atmospheric effects can affect in some cases even dramatically the quality of EO data and the effect is depended on the spectral band used (Agapiou et al., 2011). Hadjimitsis et al. (2010) highlighted a mean difference of 18% for NDVI with and without atmospheric correction implementation. On the other, in the TIR window, atmospheric transmissivity and path radiance can affect the retrieval accuracy of surface temperature by even more than 10°C (French et al., 2003). Thus, it is undoubtedly of key interest to explore the atmospheric correction effect on the "triangle"-predictions accuracy.

In purview of the above, this study's objectives are two-fold: Firstly, to explore the ability of the "triangle" in deriving spatiotemporal estimates of energy fluxes and SMC using EO data from the Advanced Along-Track Scanning Radiometer (AATSR) acquired at a range of European ecosystems. A further objective has been to assess the effect of atmospheric corrections on the technique's accuracy. For this purpose, the "triangle" was implemented at selected CarboEurope sites for which non-atmospherically corrected (AATSR 1P) and atmospherically corrected (AATSR 2P) AATSR satellite data operational products had been acquired for selected experimental days or 47 days in total spanning the period 2007-2011.

2. TRIANGLE DESCRIPTION & IMPLEMENTATION

2.1 The Ts/VI domain

Numerous investigations already published have established the physical properties embedded in the triangular (or trapezoidal) shape that emerges from a scatterplot between T_s and VI (Gillies et al., 1997; Carlson 2007; Maltese et al., 2015; Carlson & Petropoulos, 2019). This shape arises from the different effect that surface water content has on T_s, being higher over vegetated areas in contrast to bare soil areas. Such a scatterplot is characterised by four boundaries, as illustrated in **Figure 1**. The so-called "dry edge" or "warm edge" is delineated by the points of highest temperature which include a range of bare soil and vegetation fractions. Presumably, it represents circumstances of restricted surface soil water content and zero soil evaporative flux. Likewise, the "wet edge" or "cold edge" portrays the water availability in relation to vegetation conditions. Variation along the "base" of the triangle reflects the joint effect of the spatial variability in soil water and elevation. For data points with identical VI, the pixels with the minimum T_s are those with the strongest evaporative cooling, whereas the opposite is the case for the pixels with maximum T_s.

2.2 "Triangle" Implementation

The "triangle" operation links the Ts/VI scatterplot with a SVAT model which allows estimating spatially turbulent fluxes of LE and H (both instantaneous and daytime average) as well as SMC. An overview of the method implementation is furnished next, also depicted in **Figure 2**.

2.2.1 Data Pre-Processing

First, all the datasets need to be georeferenced to a common projection. Subsequently, if necessary, a masking should be implemented to remove pixels containing clouds, cloud shadows and water bodies. Then, vegetation fractional cover (F_r) is computed from the Normalised Difference Vegetation Index (NDVI, Deering et al. (1975) according to Gillies & Carlson (1995) as follows:

$$F_r = \left(\frac{NDVI - NDVI_o}{NDVI_s - NDVI_o} \right)^2 , \qquad (1)$$

where $NDVI_0$ and $NDVI_s$ are the minimum and maximum NDVI values respectively at the locations within the image, which are usually derived from the scatterplot of the T_s versus NDVI maps. This transformation allows plotting at the same scale both the simulations from the SVAT model and the EO-derived T_s.

The next step includes scaling of the surface temperature, T_s by means of:

$$T_{scaled} = \frac{T_s - T_{\min}}{T_{\max} - T_{\min}} , \qquad (2)$$

where T_s denotes the pixel temperature value within the study domain. T_{min} and T_{max} can be defined directly from the Ts/VI scatterplot and refer to the minimum and the maximum T_s for wet vegetated pixels and for the dry, bare soil respectively.

2.2.2 Coupling EO with the SVAT Model

In the next step, T_s (or equally T_{scaled}) and F_r are coupled with a SVAT model which allows deriving the LE/H fluxes and SMC spatially. In this study, SimSphere SVAT model is used for this purpose. This model is known from its initial development as the Penn-State University Biosphere-Atmosphere Modelling Scheme (PSUBAMS) (Carlson and Boland, 1978; Lynn and Carlson, 1990). SimSphere has significantly evolved by Gillies et al. (1997) and later by Petropoulos et al. (2013b) & Anagnostopoulos & Petropoulos (2017). A comprehensive overview of the SVAT model use can be found in Petropoulos et al. (2009b).

SimSphere parameterisation requires providing as input information concerning the experimental area geographical location, soil and vegetation properties as well as atmospheric profile data. Once SimSphere is parameterised, it is then iterated up to the point where the simulated (modelled with the SVAT) the extreme values of F_r and T_s as recorded from the EO data match. These conditions define the initial state of the model conditions. Then, it is iterated for all theoretical combinations of Fr and SMC (in this case in increments of 10% and 0.1 for Fr and SMC respectively) keeping all other model inputs fixed. The output values of SMC, LE, H, Ts, and Rn are recorded per iteration for the specific satellite overpass time. This results to a set of model outputs presented in the form of a matrix calculated for each set of F_r and SMC which includes the parameters SMC, F_r, T_{scaled} (or equally T_s), LE and H Next, from this matrix a series of non-linear (cubic) equations are computed, relating F_r and T_{scaled} to each of the other variables of interest: instantaneous SMC, H, LE, and also the daytime average LE and H fluxes as expressed from the ratios of LE/R_n and H/R_n respectively, where R_n is the Net Radiation (computed by the model as well). These equations are essential quadratic equations which for example, for the case of the relation of SMC to F_r and T_s and/or T_{scaled} have the form shown below:

$$SMC = \sum_{p=0}^{3} \sum_{q=0}^{3} a_{pq} (T_{scaled}{}^{*})^{p} (F_r)^{q} \quad , \qquad (3)$$

where $a_{p,q}$ are the coefficients estimated from the non-linear regression between the F_r, T_{scaled} and *SMC* while p and q vary from 0 to 3. Thus, these equations establish the physically-based simple and empirical relationships used to estimate the SMC and LE/H fluxes at the selected locations and times. The derived equations are subsequently employed to the AATSR derived Fr and Ts products in order to obtain the LE/H and SMC spatially explicit mps.

3. EXPERIMENTAL SET UP

3.1 Study Sites

A total of 12 experimental sites were chosen from the CarboEurope monitoring network; the latter is part of FLUXNET land surface parameters monitoring network (Baldocchi et al., 1996). At CarboEurope, ground data collection is based on a uniformly adopted approach at all sites, which enables data comparison. LE and H fluxes are computed using the eddy covariance technique (Aubinet et al., 2012), whereas SMC measurement is made at a minimum in the surface and root zone soil depths using standardised instrumentation across the network sites. All the measurements acquired are subject to quality-control and error correction following standardised procedures (see Aubinet et al. 2000).

Table 1 summarises our test sites key characteristics, whereas **Figure 3** shows the geographical distribution of the sites**.** The selected sites represent different ecosystem types and were chosen taking into account certain criteria. The selected test needed to belong to CarboEurope validated network and also data from the exact same processing level should be available. Sites were also chosen based on differing land cover types to allow analysis of the land cover effect on the accuracy of retrieval results. A total of 47 days of in-situ data measured at a 30' time step from each experimental site were acquired. These 47 days adequately cover the period from 2007-2011. The main criteria for selecting the specific days included as complete as possible, cloud-free, good quality *in-situ* data on which concurrent AATSR images were available from different land use/cover types. The in-situ data was acquired from FLUXNET global observational network (http://fluxnet.ornl.gov/obtain-data) at Level 2 processing level. Besides, local atmospheric profiles at 06.00 hours were acquired from the geographically nearest experimental site available in the University's of Wyoming weather archive (http://weather.uwyo.edu/upperair/sounding.html).

3.2 Satellite Observations

AATSR is a dual-view imaging radiometer on board the European Space Agency (ESA) ENVISAT satellite. It records both the reflected and emitted radiation at 7 spectral bands distributed from the optical to thermal infrared parts of the electromagnetic spectrum at a 512 km swath and a spatial resolution of 1 km at nadir and 1-3 days temporal resolution. In this study, two AATSR products were used. The first was the ATS_TOA_1P product; this is the Level 1B Product containing geolocated, radiometrically and geometrically corrected brightness temperature/radiance at the top-of-the atmosphere (TOA) projected in a longitude-latitude grid. Thermal channels include the brightness temperature at different spectral bands which has been derived from the thermal channel radiances by applying the Planck's Law. In the product, both the forward and nadir views are 'co-located' as a result of geometric correction (for more details see ESA AATSR Product Handbook, 2007). In addition, the ATS_NR_2P Level 2 geophysical product was obtained (ESA ENVISAT-1 Products Specifications Manual, 2013). This product provides the values of various geophysical parameters at 1 km spatial resolution, including the NDVI and the surface brightness temperature/radiance. All the AATSR images were acquired from ESA's EOLiSA platform (https://earth.esa.int/web/guest/eoli) for 47 days which included both the ATS_TOA_1P and ATS_NR_2P products per day.

4. METHODS

4.1 Implementation

Pre-processing of all the acquired AATSR images involved the following steps: first, the T_s, T_{BB}, radiance true values were derived by applying the scale factors provided in the ATBD of each product. Subsequently, the NDVI was computed (for the ATS_TOA_1P only) and the F_r (for both ATS_TOA_1P and ATS_NR_2P). Next, masking of clouds, and land surface covered by water and snow was applied to each image, and the product quality flags were used to remove from any further analysis spurious pixels/data. After this step, image subset was applied keeping a radius of about 50 x 50 km around each experimental site used for validation. For the ATS_TOA_1P product in particular, only the nadir views were utilized and all pre-processing steps were consequently applied to this specific dataset.

Next, the "triangle" technique was implemented for each AATSR image following the steps summarized earlier (Section 2.2.1). In addition, for each day of AATSR data, the results were recalculated using as input the F_r computed from the NDVI and the T_s which were obtained from the AATSR Surface Temperature Level 2 products (readily available in the ATS_TOA_1P product). The repetition of the calculation allowed evaluating the influence of the atmospherically corrected AASTR products on the predicted by the "triangle" LE/H fluxes and the SM, since all other inputs involved did not change for the second application of the method (using the corresponding ATS_TOA_1P product).

4.2 Statistical Analysis

Point-by-point comparisons were carried out between predicted and observed parameter values per site and also per land cover type. Degree of agreement was quantified on the basis of the statistical scores summarised in **Table 2** and a detailed description of these can be found for example in Wilmott (1982). Briefly, those statistical metrics included the linear regression coefficient of determination (R^2), the root mean square difference (RMSD), the scatter or mean standard deviation (MSD), the mean absolute difference (MAD) and the bias or mean bias error (MBE). Those statistical parameters have been used in analogous studies in the past (Brunsell and Gillies 2003; Chauhan et al., 2003) and on related operational products accuracy benchmarking studies (e.g. Validation Report Evapotranspiration Products LSA-16, 2010). The latter allowed a consistency to be maintained to previous studies and allowed a direct comparison to the results obtained in this study to previously published relevant works.

5. RESULTS

5.1 Instantaneous SMC and Turbulent Fluxes

5.1.1 SMC

In terms of the SMC comparisons (**Table 3, Figure 4a**), the agreement between the estimated and observed SMC varies significantly variations dependent on the satellite product level used in the "triangle" implementation. As demonstrated by the high R values (0.766 and 0.844 respectively), predicted and *in-situ* measurements of SMC were generally close for both the AATSR_1P (1P) and AATSR_2P (2P) implementations,. Notably, when the higher level sensor product was used, a considerable increase in correlation was evident. The 1P product exhibited a moderate overestimation of the *in-situ* measurements (MBE = 0.082 cm^3 cm^{-3}), with comparable scatter (MSD = 0.102 cm^3 cm^{-3}). The 2P product analysis reported MBE = 0.007 cm^3 cm^{-3}, an improvement in model bias prediction by 0.075 cm^3 cm^{-3} [1] and an improvement of 0.040 cm^3 cm^{-3} for scatter. Error ranges for the 1P product were relatively high, demonstrated by an RMSD of 0.131 cm^3 cm^{-3}, which exceeds by 0.031 cm^3 cm^{-3} the accuracy of 0.100 cm^3 cm^{-3} required in delivering SMC on operational status. A significant improvement in accuracy was again obtained when the 2P product was utilised in place of the lower level product. An RMSD value of 0.063 cm^3 cm^{-3} and MAD of 0.054 cm^3 cm^{-3} were exhibited for the atmospherically corrected product, an increase of 0.068 cm^3 cm^{-3} and 0.045 cm^3 cm^{-3} respectively.

With respect to land cover, correspondence between the predicted and reference SMC varied between the AATSR products (**Table 4, Figure 4a**). For the 1P product, the highest prediction performance was found for the mixed forest sites (RMSD = 0.073 cm^3 cm^{-3}). This land cover type also showed lowest bias and scatter results among all land cover types. For the 2P product, the grassland sites reported lowest RMSD of 0.057 cm^3 cm^{-3}, and a minor overestimation of the observed values (MBE = 0.008 cm^3 cm^{-3}). As evidenced in the statistical measures for all land cover types, there was significant improvement by using the 2P instead of 1P product for all land cover types. The improvement is particularly noticeable for the grassland sites (a decrease in RMSD of 0.087 cm^3 cm^{-3} from 1P to 2P). The deciduous broadleaf forest sites displayed the highest error for both product levels, with RMSD of 0.153 cm^3 cm^{-3} for the 1P and 0.084 cm^3 cm^{-3} and 2P products, respectively. RMSD results for SMC were not calculated for the cropland, evergreen needle-leaf forest and open shrubland sites due to the limited number of data sites per land cover type.

5.1.2 LE fluxes

With regards to the instantaneous LE fluxes, analysis of the 1P products returned a close correlation between the predicted and observed (R = 0.728) (**Table 3, Figure 4c**). Similarly to the SMC results, a clear and significant improvement in agreement is evident if the 2P product is utilised (R = 0.927, an increase of 0.199). Validation results also indicated that the highest correlation coefficient among all the parameters studied was obtained for the 2P LE flux implementation (R =0.919). MBE was relatively high for the 1P product (58.55 Wm^{-2}), being noticeably overestimated in comparison to the reference (i.e. *in-situ*) data. Once again, a clear improvement was displayed with the use of the atmospherically corrected product; however, results still displayed a moderate overestimation (MBE = 18.59 Wm^{-2}). Error values for the 1P product were relatively high, with both RMSD (102.21 Wm^{-2}) and MAD (80.90 Wm^{-2}) exceeding the required accuracy range for operational retrieval (50.00 Wm^{2}). In addition, moderately high scatter results suggest a relatively unstable estimate (MSD = 83.79 Wm^{-2}). If the 2P product is used, RMSD drops to 49.03 Wm^{-2} and MAD to 40.62 Wm^{-2}. Both error values achieve the required accuracy for practical application. Lower scatter values for the 2P implementation also suggest stable prediction (MSD = 45.37 Wm^{-2}).

The instantaneous LE fluxes comparisons showed large variability depending on land cover type and product level used (**Table 4, Figure 4c**). For the case of the 1P product, the closest agreement between the predictions and *in-situ* LE fluxes was found for the evergreen broadleaf forest sites (RMSD = 74.27 Wm^{-2}); these sites also exhibited the lowest bias (MBE = 19.81 Wm^{-2}). Similarly with the SMC comparisons, agreement over the mixed forest sites was also moderately close

(RMSD = 76.60 Wm^{-2}). The cropland and evergreen needle-leaf forest sites displayed very high error, with RMSD values of 120.78 Wm^{-2} and 131.50 Wm^{-2} and MAD values of 93.16 Wm^{-2} and 115.07 Wm^{-2} respectively. Regarding the comparisons for the 2P implementation, RMSD improved markedly for all land cover types. Most notably, RMSD for the evergreen needle-leaf forest sites displayed a significant drop to 5.02 Wm^{-2}. Additionally, the grassland site again exhibited high accuracy, with an RMSD of 47.03 Wm^{-2} and a MAD of 37.39 Wm^{-2}. The highest RMSD was found for the evergreen broadleaf forest and cropland sites, which displayed values of 59.75 Wm^{-2} and 56.53 Wm^{-2} respectively. However, one should keep in mind that the statistics calculated for evergreen needle-leaf forest are based on just two points and are thus most likely inaccurate. For the deciduous broadleaf forest and open shrubland sites no results were reported for LE flux comparisons due to absence of data points. Overall, as shown in Table 4, the sample sizes are small. Therefore, a goal of future studies should be to examine the relation between estimates and observations based on larger sample sizes.

5.1.3 H fluxes

Correspondence between the 1P "triangle" H flux predictions and the reference data from CarboEurope sites was relatively low for the instantaneous H flux comparisons, as evidenced by the correlation coefficient results (R - 0.305) (**Table 3, Figure 4b**), which notably, was the lowest of all parameters. There was a clear difference in agreement between the two AATSR product levels, with the 2P product showing an improvement in R of 0.382, increasing to 0.687. The 2P implementation also showed a minor improvement in estimation bias in comparison to the results of the 1P (an improvement of 0.74 Wm^{-2} in MBE). Notably, that the 2P product underestimated the *in-situ* measurements (MBE = -11.15 Wm^{-2}), in contrast to the positive bias shown by the 1P product (MBE = 11.89 Wm^{-2}). Interestingly, the only 3 instances of underestimation by the model predictions were all recorded for either the instantaneous or daytime average H flux parameter comparisons. RMSD for both product levels were comparable, with only a minor improvement between the accuracy of validation results of both products (1P RMSD= 63.24 Wm^{-2}/2P RMSD = 44.37 Wm^{-2}).

In regards to the comparisons of the predicted H fluxes over different land cover types, those show overall better agreement between observations and model-based estimates than the LE fluxes results (**Table 4, Figures 4b and 4c**). For the 1P product, the lowest RMSD was exhibited for the cropland sites (RMSD = 16.99 Wm^{-2}), with comparable values between the other land cover types (RMSD = 59.69 – 81.44 Wm^{-2}). Similarly with the LE fluxes comparisons, the highest RMSD was displayed by the evergreen needle-leaf sites (RMSD = 81.44 Wm^{-2}). Regarding the results of the 2P product, the cropland sites showed a decline in accuracy of ~46% compared to the 1P product; this result is in contrast with all other land cover types which showed an improvement between 19.31 and 38.62 Wm^{-2}. In contrast to the LE comparisons, the highest error value was found for the evergreen needle-leaf forest sites (RMSD = 55.96 Wm^{-2}). Results for the evergreen broadleaf forest, mixed forest and open shrubland sites were unavailable for H flux comparisons due to limited sample size.

5.2 Daytime Energy Fluxes

The performance of the daytime average LE and H heat flux estimates, expressed by the ratios of LE/R_n and H/R_n respectively, was poor in comparison to the results reported for the instantaneous fluxes (**Table 3, Figure 5**). Agreement between both datasets was low for the 1P product, exhibited by R values of 0.494 and 0.572 for the LE/R_n and H/R_n parameters respectively. An improvement was evident when the 2P product was utilised (improvement of

0.140 and 0.066 for the LE/R_n and H/R_n respectively). For both the 1P and 2P product implementations, the predicted LE/R_n estimations systematically overestimated the *in-situ* data (MBE 1P = 0.102/MBE 2P = 0.042), while for the H/R_n parameter the model-based estimates underestimated the data (MBE 1P = -0.024/MBE 2P = -0.038). A clear improvement in RMSD was obtained for both parameters by using the level 2P product as seen in Table 3. It should be noted that all daytime averaged scenarios failed to reach the required accuracy of RMSD=0.100 cm^3 cm^{-3} for operational application.

The statistical analyses concerning the daytime fluxes agreement over different land cover types also showed relatively low prediction accuracy in comparison to both the instantaneous LE and H fluxes results (**Table 5, Figures 4b-4c and Figures 5a-5b**). The RMSD for the 1P product comparisons ranged from 0.159 for the mixed forest, to 0.264 for the evergreen needle-leaf sites. Some similarities were apparent between the instantaneous and daytime averaged LE fluxes results, with the mixed forest performing relatively well and the highest error rates being associated with the evergreen needle-leaf sites. Improvement in agreement over all sites was evident when the 2P product was used. Most noticeable improvement in RMSD was shown for the evergreen needle-leaf forest sites (improved from 0.264 to 0.057), in agreement with the instantaneous results. Results were again generally poor for the daytime-averaged H fluxes for all types of land cover included. Lowest RMSD for the 1P product implementation correlated with the instantaneous H flux results (cropland RMSD = 0.086), with the remaining land cover types ranging from 0.113 to 0.223. In contrast to the results for other parameters , error values only showed improvement for 2 of the 7 land cover types (deciduous broadleaf forest and evergreen broadleaf forest sites) when the 2P product was utilised, with the remaining 3 (open shrubland, evergreen needle-leaf and cropland sites) showing a decline in accuracy between 0.001 and 0.057. Results for the grassland and mixed forest sites were unavailable for daytime average H flux comparisons due to limited data points.

6. DISCUSSION

This study was concerned with a robust verification of the so-called “triangle” technique implemented with AATSR level 1 and 2 products was performed. The reference data was obtained from 12 CarboEurope sites for 47 selected days during the period 2007-2011. Overall, results suggested that estimates of energy fluxes and SMC by the investigated method utilising the lower-level 1P product yielded moderate accuracies. The integration of the higher level AATSR_2P product significantly improved the accuracy, leading to estimates, for the majority of the studied parameters that achieve the required accuracy for many practical applications. Improvements were evident in almost all statistical comparison measures if the higher level 2P product is used which has undergone a more extensive pre-processing.

SMC results were comparable to those reported in the limited number of similar studies available in the literature. For example, Capehart and Carlson (1997) implemented the “triangle” with EO data from the Advanced Very High Resolution Radiometer (AVHRR) data. Authors compared the predicted SMC from the technique versus simulations from a soil hydrological model and reported a RMSD varying from 0.15 to 0.19 respectively and a low correlation (R^2 from 0.266 to 0.441). Authors attributed the relatively low agreement in SMC to the mismatch between the hydrological model and the EO data arguing that the “triangle”-predicted SMC may respond to water content a much shallower soil layer in comparison to the hydrological model. Gillies et al. (1997) implemented the “triangle” also with airborne data from the NS001 multispectral scanner and reported R^2 ranging between 0.29 to 0.79 and standard errors varying from 8.73 to 8.25 %, results comparable to those reported herein.

To our knowledge, very few studies have explored the “triangle” integrated with a land biosphere model, and thus direct comparisons of the results presented here to such studies are not available. However, a number of recent variants of the “triangle” have evaluated the effect of using different inputs to construct the T_s/VI feature space and thus derive SMC from newly proposed indices. For example, Chauhan et al. (2003) using satellite observations from the Advanced Very High Resolution Radiometer (AVHRR) and the Special Sensor Microwave Imager (SSM/I) implemented a variant of the “triangle” for an experimental area in Southern Great Plains. Authors reported a RMSD below that 0.05 cm^3 cm^{-3} in the prediction of SMC by their technique. Yet, results of their study would be inappropriate scientifically to be directly compared to our study due to differences in the testing conditions (e.g. in their study test sites were covered by bare soil only). In a different study, Zhang et al. (2014a) proposed estimating SMC from the mid-morning Ts increase rate using the so-called Temperature Rising Rate Vegetation Dryness Index (TRRVDI) to construct the Ts/VI feature space. Authors implemented their proposed scheme using Meteosat Second Generation (MSG) Spinning Enhanced Visible and Infrared Imager (SEVIRI) EO data acquired over an experimental site in Spain that contained data from 19 meteorological stations and found a mean R^2 and RMSD of 0.46 and 4% cm^3 cm^{-3} respectively, results analogous to our findings. Zhang et al. (2014b) also utilised MSG SEVIRI to implement a variant of the “triangle”, termed the Soil Moisture Saturation Index (SMSI), to estimate SMC. The SMSI was estimated from the Ts/VI feature space using EO data from the Apparent Thermal Inertia (ATI) in place of both LST and F_r. Authors reported an R of 0.33 and 0.43 for SMC, agreement that is below what was found herein. Authors suggested that spatial scale discrepancies and the fact that ATI is an accumulation of multi-surface interactions compared to single-surface SMC recorded by the *in-situ* stations were potential reasons for poorer agreement.

In regards to the LE fluxes predictions, results were in close agreement to other studies as well. For example, Gillies et al. (1997) compared the LE predicted by the triangle versus ground observations from FIFE (Sellers et al., 1992) and MONSOON’90 (Kustas and Goodrich, 1994) field experiments using data from the NS001airborne scanner (30 m spatial resolution) and found a mean standard error of 34.73 Wm^{-2} in LE prediction. In another study, Brunsell and Gillies (2003) implemented the “triangle” with both airborne (from TIMS sensor) and satellite (from NOAA AVHRR) data acquired during the SGP’97 Hydrology experiment. They reported an RMSD ranging from 18 to 90 Wm^{-2}. More recent studies have concentrated on developing variants of the “triangle” to estimate LE flux. For example, Batra et al., (2006) presented results of an extensive inter-comparison of variants of “triangle”-derived spatially distributed LE fluxes, based on data from MODIS, AVHRR, NOAA14 and NOAA16 sensors. Validation against ground stations in the SGP region displayed RMSDs ranging from 51 to 73 Wm^{-2}, comparable to results presented in this study. In a different study, Bhattacharya et al., (2010) utilised Kalapana-1 VHRR (K1VHRR) Indian geostationary sensor to estimate regional clear sky ET and LE flux. RMSD was again comparable with 46 Wm^{-2} with an R value of 0.610.

The predicted H fluxes reported herein are also comparable to prior verification exercises of the “triangle” technique implemented using dissimilar EO data. Gillies et al. (1997) validated the technique using the NS001 multispectral scanner airborne data and found for H fluxes a R^2 of 0.83 and standard errors of ranging from 25 to 55 Wm^{-2}. Brunsell (2003) and Brunsell and Gillies (2003) also implemented the “triangle” method with high resolution airborne from TIMS sensor and also with AVHRR data acquired during the SGP ’97 field experiment in the USA. They reported a agreement in H fluxes varying from 21 to 145 Wm^{-2} for the AVHRR comparisons and between 45 to 80 Wm^{-2} for the TIMS data. Tang et al., (2010) implemented the “triangle” in a north western region of China using the MODIS land surface temperature/emissivity (MOD11) and NDVI

(MOD13) products. Authors reported in their study a RMSD of 25.07 Wm^{-2} in H flux estimation. Tang et al., (2010) attributed as one of the main error causes the lack of available uncontaminated points on partly cloudy days.

Daytime average H and LE fluxes predictions were closely tied to the instantaneous H and LE fluxes predictions. This observation is in line to findings reported by others concerned with the method verification (Gillies et al., 1997 and Brunsell and Gillies, 2003). Generally, LE and LE/R_n were in closer agreement to the reference data in comparison to the derived H and H/R_n fluxes. The latter may be due to the prediction accuracy of SimSphere itself in terms of predicting itself those parameters, as found in verification studies of the model itself (e.g. North et al., 2015). Unfortunately, no other studies had previously assessed the "triangle" with respect to the prediction of the daytime averaged fluxes. However, notably, prediction accuracy of both daytime fluxes is comparable to the retrieval accuracy of other methods used in deriving these parameters, as for example approaches utilising the evaporative fraction (EF) (Jiang and Islam, 2003; Nishida et al., 2003; Wang et al., 2006), although we underline that a direct assessment of the different methods would not be suitable.

Ideally issues related to all significant error sources should be taken into account in interpreting this study's main findings (Gillies et al., 1997; Brunsell and Gillies, 2003; Chauhan et al., 2003). Errors in the EO data, related to both the accuracy in which F_r and T_s/T_{kin} retrievals are derived and also potentially linked to the spatial resolution mismatch between the *in-situ* and predictions, can potentially significantly affect the accuracy of "triangle" predictions. As it has already been pointed out in several T_s/VI studies an improved accuracy in the estimation of T_s would be expected to also improve the "triangle" estimates (Gillies and Temesgen 2000; Islam et al., 2003). F_r has also been found to importantly contribute to the overall sensitivity of parameters computed in SimSphere, thus supporting the inclusion of this parameter in the "triangle" (e.g. Petropoulos et al., 2014). Hence, errors in F_r retrieval from the EO data may have an important effect on the accuracy of the predictions and subsequently lead to uncertainties in the inversion equations computed for all the predicted parameters by the technique. The effect of atmospheric correction of the EO inputs is also a factor to be considered in the "triangle", at least this was the case herein.

Explanation of results based on comparing directly the in-situ measurements with the EO data should be cautiously interpreted; this is because such a comparison may be limited by factors such as scale mismatch, geo-location errors and errors introduced as a result of the surface heterogeneity, with the latter being dependent also on the spatial resolution of the EO dataset (Batra et al., 2006; Bhattacharya et al., 2010). Due to the significant difference in spatial resolution between the CarboEurope point measurements (in the order of 5 × 5 m), and the AATSR satellite pixel (in the order of 1 × 1 km), a direct validation is subject to uncertainty caused by the scale effect (Capehart and Carlson, 1997; Stisen et al., 2008). Furthermore, agreement between the *in-situ* data and the predictions are not only hindered by horizontal spatial discrepancies, but also by vertical discrepancies in the derivation of the parameters. In particular, *in-situ* monitoring networks, such as CarboEurope, normally measure SMC as an average derived from the top 0-5 cm of the soil, whereas the "triangle" predicts the soil water content availability, the latter being a parameters that can be converted to SMC if knowing the soil's field capacity. Another consideration for interpreting the results is related to the uncertainty in the *in-situ* observations, due to instrumentation uncertainty or error. Uncertainty in turbulent flux measurement by means of the eddy covariance system is typically in the order of 10-15 % (Dugas et al., 1991), and can potentially increase if the eddy covariance system is installed in non-flat terrain (Schmid and Lloyd, 1999).

7. CONCLUSIONS

This study investigated, to our knowledge for the first time, the implementation of the so-called "triangle" technique with EO data from ESA's AATSR sensor to derive LE/H fluxes and SMC over a range of European ecosystems. Furthermore, for the first time was also evaluated the atmospheric correction effect on the "triangle"-derived retrievals. For this purpose, both non-atmospherically corrected and atmospherically corrected AATSR data were used to implement the "triangle". Predicted LE and H fluxes and SMC were statistically compared versus collocated ground measurements acquired at a variety of CarboEurope study sites.

In overall, results showed a satisfactory agreement between the *in-situ* and both "triangle" schemes in terms of SMC prediction (1P: R = 0.766 vs 2P: R= 0.844). Instantaneous LE and H fluxes predicted by the "triangle" were again much improved with the inclusion of the atmospherically corrected 2P product. The statistical analysis of the daytime average LE and H heat fluxes, were generally of lower accuracy compared to the validation accuracies exhibited by both the instantaneous LE and H fluxes (RMSD values of 0.146 and 0.130 and R values of 0.635 and 0.638 for the 2P comparisons for LE/R_n and H/R_n respectively). Furthermore, findings of this study also provide an important evaluation of the importance of atmospheric correction on remotely sensed datasets before the latter are used as inputs in the "triangle". In particular, results suggest that ensuring that true surface reflectance values are determined through full atmospheric correction is an invaluable step before deriving sensor-based images of T_s and NDVI and implementing the "triangle" technique.

Although AATSR no longer provides data, it does provide a direct link to present work on the operational retrieval of surface fluxes and SMC that is carried out on current sensors (e.g. Landsat 8, MODIS, Sentinels-3) and on other EO instruments with similar characteristics that may be planned for launch in the near future. This offers an avenue for the transfer of such methodologies to current and future operational platforms. An example is ESA's Sentinel-3 mission, which makes use of both the on-board Sea and Land Surface Temperature Radiometer (SLSTR) and Ocean and Land Colour Instrument (OLCI) radiometers to offer data continuity for the AATSR instrument. Both platforms have similar spatial resolution and the swaths of the two sensors overlap, permitting for novel joint applications or easy transferability between the two sensors. Thus, validation of the "triangle" utilising AATSR data provides an opportunity to assess the viability of extending it to newer platforms for more up-to-date research. Last but not least, our results are of considerable technical and practical significance in regards to the "triangle" technique use in the future, especially in light of ongoing efforts that aim to assess its application for operational product development at global scale.

Acknowledgments

Dr Petropoulos participation to this study was funded under the Marie Skłodowska-Curie ENVISION project (grant agreement No 752094), funded by the European Union's Horizon 2020 research and innovation programme. We would also like to thank the CarboEurope principal investigators for the free access to the ground measurements. Also, we would like to thank ESA, since initial acquisition of most of the EO data and their pre-processing as used in this study had been performed during the ESA-funded PROgRESSIoN project.

Declaration of Interest

The authors declare that they have no conflict of interest.

References

Agapiou A., Hadjimitsis D.G., Papoutsa C, Alexakis D.D., Papadavid G., 2011. The importance of accounting for atmospheric effects in the application of NDVI and interpretation of satellite imagery supporting archaeological research: the case studies of Palaepaphos and Nea Paphos sites in Cyprus. Remote Sensing 3(12):2605-2629.

Anagnostopoulos, V., Petropoulos, G.P., 2017. A Modernized Version of a 1D Soil Vegetation Atmosphere Transfer model for Use in Land Surface Interactions Studies. Environmental Modelling & Software, 90 pp. 147-156.

Aubinet M, Grelle A, Ibrom A., Rannik Ü., Moncrieff J., Foken T., ... Vesala T., 2000. Estimates of the annual net carbon and water exchange of forests: the EUROFLUX methodology 30:113-175.

Aubinet, M., Vesala, T., Papale, D. (Eds.), 2012. Eddy Covariance: A Practical Guide to Measurement and Data Analysis. Springer Atmospheric Sciences, Springer Verlag, 438 pp.

Baldocchi D.D., Valentini R., Running SR., Oechel W., Dahlman R., 1996. Strategies for measuring and modeling carbon dioxide and water fluxes over terrestrial ecosystems. Global Change Biology 2:159–168.

Bao, Y., Lin, L., Wu, S., Deng, K.A.K., Petropoulos, G.P., 2018. Surface Soil Moisture Retrievals Over Partially Vegetated Areas From the Synergy of Sentinel-1 & Landsat 8 Data Using a Modified Water-Cloud Model. International Journal of Applied earth Observation & Geoinformation, 72, 76-85, /doi.org/10.1016/j.jag.2018.05.026

Bao, Y., Lin, L., Wu, S., Deng, K.A.K., Petropoulos, G.P., 2018. Surface Soil Moisture Retrievals Over Partially Vegetated Areas From the Synergy of Sentinel-1 & Landsat 8 Data Using a Modified Water-Cloud Model. International Journal of Applied earth Observation & Geoinformation, 72, 76-85, /doi.org/10.1016/j.jag.2018.05.026.

Batra N,, Islam S,, Venturini V,, Bisht G,, Jiang LE., 2006. Estimation and comparison of evapotranspiration from MODIS and AVHRR sensors for clear sky days over the Southern Great Plains. Remote Sensing of Environment 103(1):1-15.

Brunsell N,A, Gillies R,R., 2003. Scale issues in land-atmosphere interactions: implications for remote sensing of the surface energy balance. Agricultural and Forest Meteorology 117:203-221.

Brunsell N,A., 2003. An examination of scale issues involved with Remotely Sensed data. PhD Thesis, University of Utah, USA.

Byun K,, Liaqat U,W., Choi M., 2014. Dual-model approaches for evapotranspiration analyses over homo-and heterogeneous land surface conditions. Agricultural and Forest Meteorology 197:169-187.

Capehart W,J., Carlson T,N., 1997. Decoupling of surface and near-surface soil water content: a remote sensing perspective. Water. Resour. Res. 33(6):1383-1395.

Carlson T.N., 2007. An overview of the "triangle method" for estimating surface evapotranspiration and soil moisture from satellite imagery. Sensors 7:1612-1629.

Carlson, T.N., Petropoulos, G.P., 2019. A New Method for Estimating of Evapotranspiration and Surface Soil Moisture from Optical and Thermal Infrared Measurements: The Simplified Triangle. International Journal of Remote Sensing, DOI: 10.1080/01431161.2019.1601288, [in press]

Chauhan N.S., Miller S., Ardanuy P., 2003. Spaceborne soil moisture estimation at high resolution: a microwave-optical/IR synergistic approach. International Journal of Remote Sensing 22:4599-46.

Deering D.W., Rouse J.W., 1975. Measuring 'forage production' of grazing units from Landsat MSS data. In International Symposium on Remote Sensing of Environment, 10 th, Ann Arbor, Mich pp. 1169-1178.

Deng, K.A.K., Lamine, S., Pavlides, A., Petropoulos, G.P., Srivastava, P.K., Bao, Y., Hristopulos, D., Anagnostopoulos, V., 2019. Operational Soil Moisture from ASCAT in Support of 2 Water Resources Management. Remote Sensing MDPI, 11, 579.

Dugas, W. A., Fritschen, L. J., Gay, L. W., Held, A. A., Matthias, A. D., Reicosky, D. C., ... Steiner, J. L., 1991. Bowen ratio, eddy correlation, and portable chamber measurements of sensible and latent heat flux over irrigated spring wheat. Agricultural and forest meteorology, 56(1), 1-20.

European Space Agency, 2007. AATSR Product Handbook. Available at: https://earth.esa.int/handbooks/aatsr/CNTR.htm

European Space Agency, 2013. ENVISAT-1 Products Specifications - AATSR Products SpecificationS. Available at: https://earth.esa.int/documents/10174/437508/Vol-07-Aats-4C.pdf.

Fan, K., Zhang, Q., et al., 2019. Spatiotemporal impact of soil moisture on air temperature across the Tibetan plateau. Science of the Total Environment, 649, 1338-1348.

French A.N., Norman J.M., Anderson, M.C., 2003. A simple and fast atmospheric correction for spaceborne remote sensing of surface temperature. Remote sensing of environment 87(2):326-333.

Gillies R.R., Carlson T.N., Cui J., Kustas W.P., Humes K.S., 1997. Verification of the “triangle” method for obtaining surface soil water content and energy fluxes from remote measurements of the Normalized Difference Vegetation Index NDVI and surface radiant temperature. International Journal of Remote Sensing 18:3145–3166.

Gillies R.R., Temesgen, B., 2000. Thermal Remote Sensing in Land surface Processes:160-183.

Gillies RR, Carlson TN. 1995. Thermal remote sensing of surface soil water content with partial vegetation cover for incorporation into climate models. Journal of Applied Meteorology 34(4):745-756.

Global Climate Observing System, 2010. Implementation Plan for the Global Observing System for Climate In Support Of the UNFCCC. [pdf] World Meteorological Organization. Available at: http://www.wmo.int/pages/prog/gcos/Publications/gcos-138.pdf [Accessed 22 September 2014].

Hadjimitsis, D.G., Papadavid, G., Agapiou, A., Themistocleous, K., Hadjimitsi, M.G., Retalis, A., Michaelides, S., Chrysoulakis, N., Toulios, L., Clayton, CRI., 2010. Atmospheric correction for satellite remotely sensed data intended for agricultural applications: impact on vegetation indices. Natural Hazards and Earth System Science 10(1):89-95

Holzman, M.E., Rivas, R., Piccolo, M.C., 2014. Estimating soil moisture and the relationship with crop yield using surface temperature and vegetation index. International Journal of Applied Earth Observation and Geoinformation 28:181-192.

Jiang, L., 2000. Estimation of land surface evaporation map over large areas using remote sensing data. PhD Thesis, University of Cincinnati, USA.

Jiang, L., Islam, S., 2003. An intercomparison of regional heat flux estimation using remote sensing data. International Journal of Remote sensing 24:2221-2236.

Kustas, W.P., Goodrich, D.C., 1994. Preface. MONSOON'90 Multidisciplinary Experiment. Water Resources Research 30(5):1211-1225.

Li, Z.L., Tang, R., Wan, Z., Bi, Y., Zhou, C., Tan, B., Yan, G., Zhang, X.. 2009. A review of current methodologies for regional evapotranspiration estimation from remotely sensed data. Sensors(5):3801-3853

Lu, J., Tang, R., Shao, K., Li, Z.L., Zhou, G., 2015. Assessment of two temporal-information-based methods for estimating evaporative fraction over the Southern Great Plains. International Journal of Remote Sensing, (ahead-of-print):1-17.

Lynn, B.H., Carlson, T.N., 1990. A stomatal resistance model illustrating plant vs. external control of transpiration. Agricultural and Forest Meteorology 52(1):5-43.

Maltese, A., Capodici, F., Ciraolo, G., Loggia, G.L., 2015. Soil Water Content Assessment: Critical Issues Concerning the Operational Application of the Triangle Method. Sensors 15(3): 6699-6718.

Nishida, K., Nemani, R., Glassy, J., Running, S., 2003. Development of an evapotranspiration index from Aqua/MODIS for monitoring surface moisture status, IEEE Trans. Geoscience And Remote Sensing 41(2):493-501.

North, M. R., Petropoulos, G.P., Rentall, D.V., Ireland, G.I., McCalmont, J.P., 2015. Appraising the capability of a land biosphere model as a tool in modelling land surface interactions: results from its validation at selected European ecosystems. Earth Surface Dynamics Discussions, 6, pp:217-265, DOI: 10.5194/esdd-6-217-2015.

Petropoulos GP, Griffiths HM, Dorigo W, Xaver A, Gruber A., 2013. Surface Soil Moisture Estimation: Significance, Controls, and Conventional Measurement Techniques, in: Remote Sensing of Energy Fluxes and Soil Moisture Content CRC Press, 20.

Petropoulos, G.P., Carlson, T.N., 2011. Retrievals of turbulent heat fluxes and soil moisture content by Remote Sensing, in: Advances in Environmental Remote Sensing: Sensors, Algorithms, and Applications, Taylor and Francis, 556:667–502.

Petropoulos, G.P., Carlson, T.N., Wooster, M.J., Islam, S., 2009a. A Review of Ts/VI Remote Sensing Based Methods for the Retrieval of Land Surface Fluxes and Soil Surface Moisture Content. Advances in Physical Geography 33(2):1-27.

Petropoulos, G.P., Carlson, T.N., Wooster., M.J.., 2009b. An Overview of the Use of the SimSphere Soil Vegetation Atmosphere Transfer (SVAT) Model for the Study of Land-Atmosphere Interactions. Sensors, 2009, 9(6), 4286-4308, DOI 10.3390/s90604286.

Petropoulos, G.P., Griffiths, H.M., Carlson, T.N., Ioannou-Katidis, P., Holt, T., 2014. SimSphere model sensitivity analysis towards establishing its use for deriving key parameters characterising land surface interactions. Geoscientific Model Development 7(5):1873-1887.

Petropoulos, G.P., Griffiths, H.M., Tarantola, S., 2013b. A sensitivity analysis of the SimSphere SVAT model in the context of EO-based operational products development. Environmental Modelling & Software 49:166-179.

Petropoulos, G.P., Ireland, G., Barrett, B., 2015. Surface soil moisture retrievals from remote sensing: Current status, products & future trends. Physics and Chemistry of the Earth, Parts A/B/C.

Petropoulos, G.P., Ireland, G., Lamine, S., Ghilain, N., Anagnostopoulos, V., North, M.R., Srivastava, P.K., Georgopoulou, H., 2016. Evapotranspiration Estimates from SEVIRI to Support Sustainable Water Management. Journal of Applied Earth Observation & Geoinformation, 49, 175-187, DOI 10.1016/j.jag.2016.02.006.

Petropoulos, G.P., McCalmont, J.P., 2017. An Operational In-situ Soil Moisture and Soil Temperature Monitoring Network for West Wales, UK: The WSMN network. Sensors,17, pp:1481-1491, doi:10.3390/s17071481

Petropoulos, G.P., Srivastava, P.K,. Feredinos, K.P., Hristopoulos, D., 2018a. Evaluating the capabilities of optical/TIR imagine sensing systems for quantifying soil water content. Geocarto International, DOI 10.1080/10106049.2018.1520926

Petropoulos, G.P., Srivastava, P.K., Piles, M., Pearson, S., 2018b.: EO-based Operational Estimation of Soil Moisture and Evapotranspiration for Agricultural Crops in Support of

Sustainable Water Management. Sustainability MDPI, 10, 181-1-20, doi:10.3390/su10010181

Piles, M., Camps, A., Vall-Llossera, M., Corbella, I., Panciera, R., Rüdiger, C., ... & Walker, J., 2011. Downscaling SMOS-derived soil moisture using MODIS visible/infrared data. Geoscience and Remote Sensing, IEEE Transactions on 49(9):3156-3166.

Piles, M., Petropoulos, G.P., Sanchez, N., González-Zamora, A., Ireland, G., 2016. Towards Improved Spatio-Temporal Resolution Soil Moisture Retrievals From the Synergy of SMOS & MSG SEVIRI Spaceborne Observations. Remote Sensing of Environment, 180, pp:403-471, DOI 10.1016/j.rse.2016.02.048.

Schmid, H.P., Lloyd, C.R., 1999. Spatial representativeness and the location bias of flux footprints over inhomogeneous areas. Agricultural and Forest Meteorology 93(3):195-209.

Sellers, P., Hall, F.G., Asrar, J., Strubel, D.E., Murthy, R.E., 1992. An overview of the First Intenational Satellite Land Surface Climatology project (ISLSCP) Field Experiment (FIFE). Journal of geophysical research 97:18345-18371.

Seneviratne, I.S., Corti, T., Davin, E.L., Hirschi, M., Jaeger, E.B., Lehner, I., Orlowsky, B., Teuling, A.J., 2010. Investigating soil moisture-climate interactions in a changing climate: a review. Earth Sci. Rev. 99, 125–161.

Sentinel 3, 2015. ESA Earth Online. [online] Available at: https://earth.esa.int/web/guest/missions/esa-future-missions/sentinel-3 [Accessed 10 July 2015].

Shi, Q., Liang, S., 2014. Surface-sensible and latent heat fluxes over the Tibetan Plateau from ground measurements, reanalysis, and satellite data. Atmospheric Chemistry and Physics 14(11):5659-5677.

Silva-Fuzzo, D., Carlson, T.N., Kourgialas, N., Petropoulos, G.P., 2019. Coupling Remote Sensing with a water balance model for soybean yield predictions over large areas. Earth Science Informatics, doi.org/10.1007/s12145-019-00424-w.

Srivastava, P.K., Han, D., Islam, T., Petropoulos, G.P., Gupta, M., Dai, Q., 2016. Seasonal evaluation of Evapotranspiration fluxes from MODIS Satellite and Mesoscale Model Downscaled Global Reanalysis Datasets. Theoretical and Applied Climatology, pages 1-14, DOI 10.1007/s00704-015-1430-1.

Srivastava, P.K., Pandley, P. C., Petropoulos, G.P., Kourgialas, N. K., Pandey, S., Singh, U., 2019. GIS and remote sensing aided information for soil moisture estimation: A comparative study of interpolation technique. Resources MDPI, 8, 70, DOI: 10.3390/resources8020070

Stisen, S., Sandholt, I., Nørgaard, A., Fensholt, R., Jensen, KH., 2008. Combining the triangle method with thermal inertia to estimate regional evapotranspiration—Applied to MSG-SEVIRI data in the Senegal River basin. Remote Sensing of Environment 112(3):1242-1255.

Stoyanova, J. S., Georgiev, C. G., 2013. SVAT modelling in support to flood risk assessment in Bulgaria, Atmos. Res., 123, 384-399.

Sun, P. Y., Wu, J. Xiao, J., Hui, J., Hu, F., Zhao, L., Qiu, Liu, S., 2019. Remote sensing and modeling fusion for investigating the ecosystem water-carbon coupling processes, Science of the Total Environment, 1340-64, https://doi.org/10.1016/j.scitotenv.2019.134064.

Tang. R., Li, Z.L., Tang, B., 2010. An application of the Ts-VI triangle method with enhanced edges determination for evapotranspiration estimation from MODIS data in arid and semi-arid regions: Implementation and validation. Remote Sensing of Environment 114(3):540-551.

Thoma, D.P., Moran, M.S., Bryant, R., Rahman, M.M., Collins, C.D., Keefer, T.O., Noriegac, R., Osmand, I., Skrivina, S.M., Tischlere, M.A., Boschf, D.D., Starksg, P.J., Peters-Lidard CD., 2008. Appropriate scale of soil moisture retrieval from high resolution radar imagery for bare and minimally vegetated soils. Remote Sensing of Environment 112(2):403-414.

Validation Report Evapotranspiration Products LSA-16 (MET), LSA (DMET), 2010. Doc Number, SAF/LAND/RMI/VR/06. Available at: http://landsaf.meteo.pt/GetDocument.do;jsessionid=958890883 1FFC55ECD304FB798539712?id=309 [Accessed on 01/09/2011].
Vereecken, H., Huisman, J.A., Pachepsky, Y., Montzka, C., van der Kruk J, Bogena H, Weihermüller L, Herbst M, Martinez G, Vanderborght J., 2014. On the spatio-temporal dynamics of soil moisture at the field scale. Journal of Hydrology 516:76-96.
Wang, K., Li Z., Cribb, M., 2006. Estimation of evaporative fraction form a combination of day and night land surface temperatures and NDVI: A new method to determine the Priestley-Taylor parameter. Remote Sensing of Environment 102:293-305.
Willmott C.J. 1982. Some comments on the evaluation of model performance. Bulletin of the American Meteorological Society 63(11):1309-1313.
Wood, E.F., Roundy, J.K., Troy, T.J., Van Beek, L,.P.H., Bierkens, M.F., Blyth, E., Whitehead, P., 2011. Hyperesolution global land surface modelling: Meeting a grand challenge for monitoring Earth's terrestrial water. Water Resources Research, 47(5).

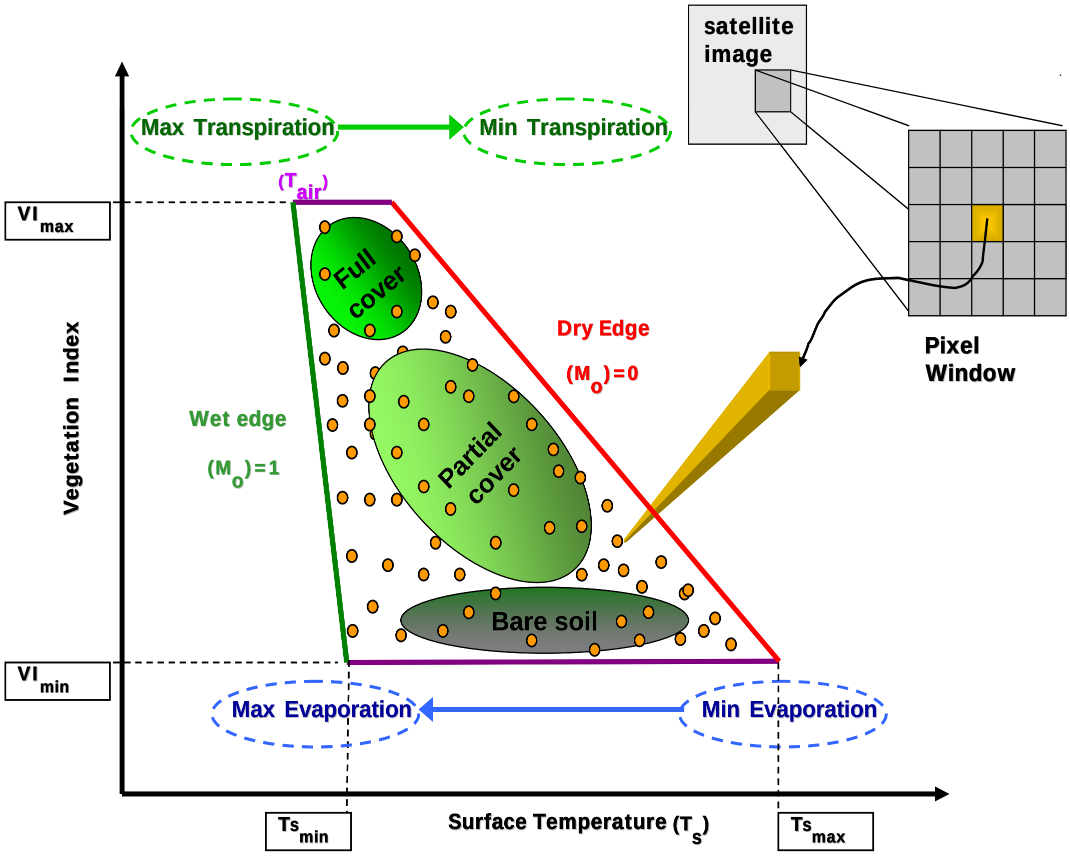

Figure 1: *Summary of the key descriptors and physical interpretations of the T_s/VI feature space "scatterplot". Figure adopted from Petropoulos et al. (2009).*

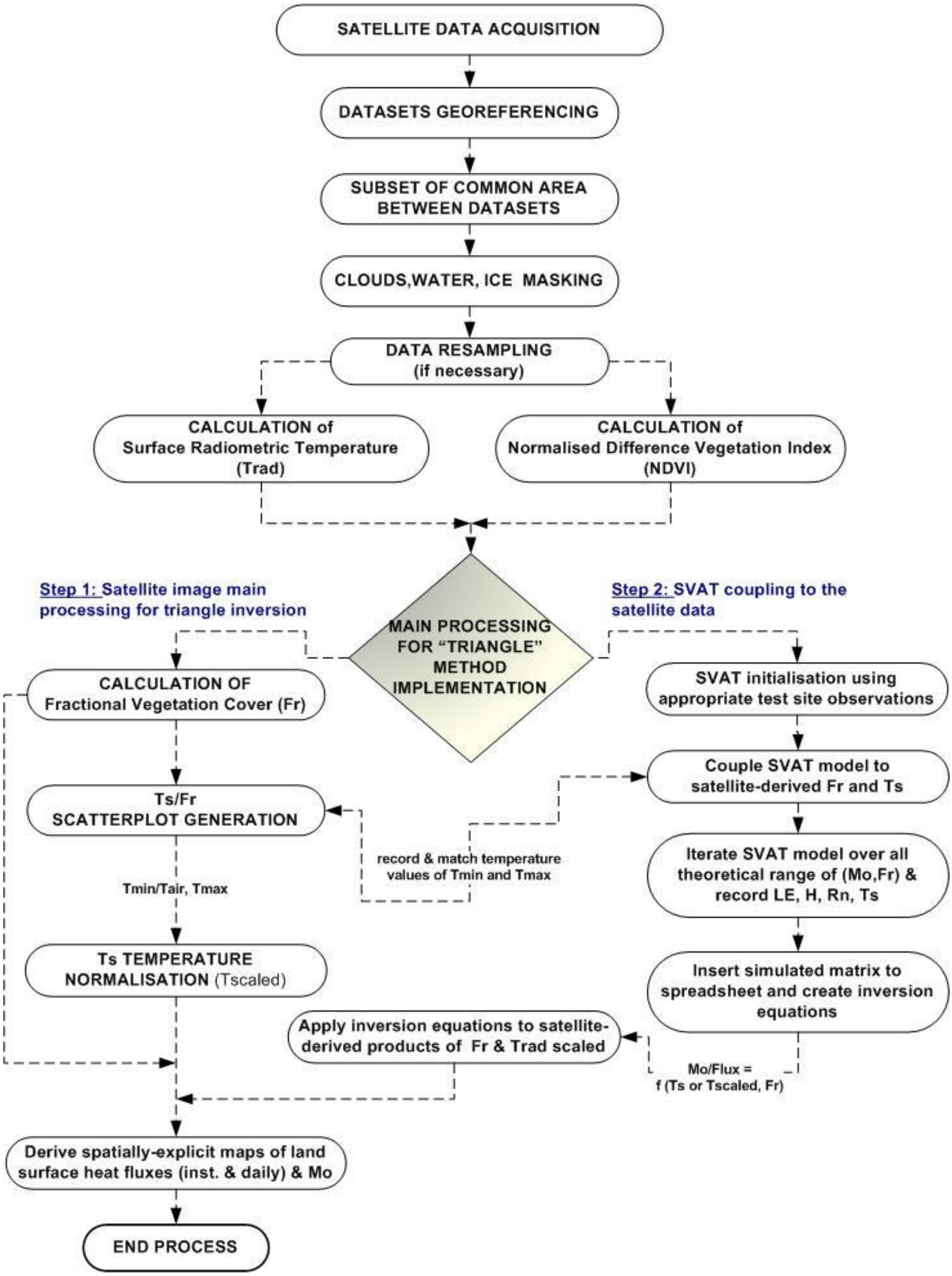

Figure 2: *Overview of the steps comprising the "triangle" technique implementation.*

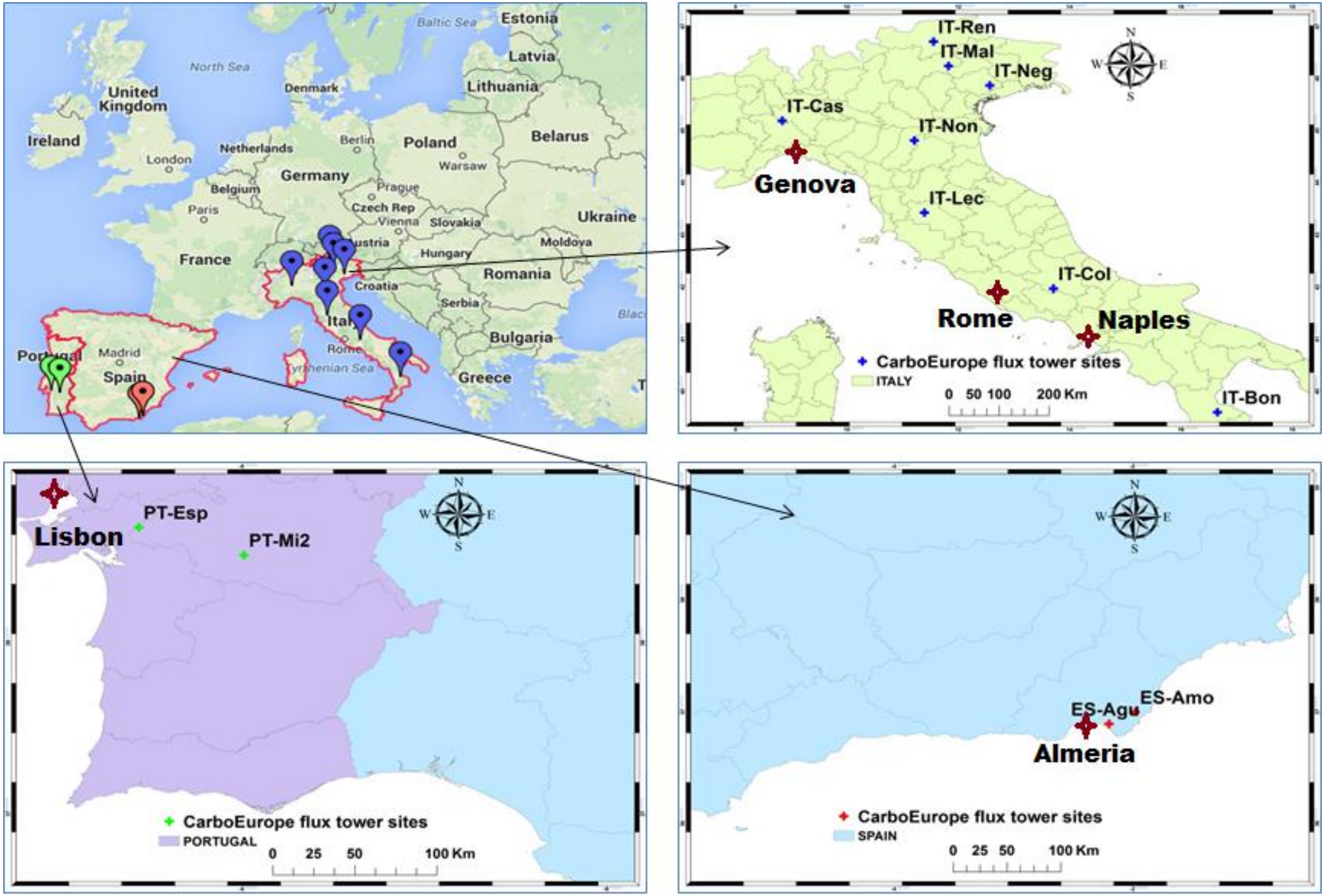

Figure 3: *Location of the study sites used in this study (Image acquired from Google Earth).*

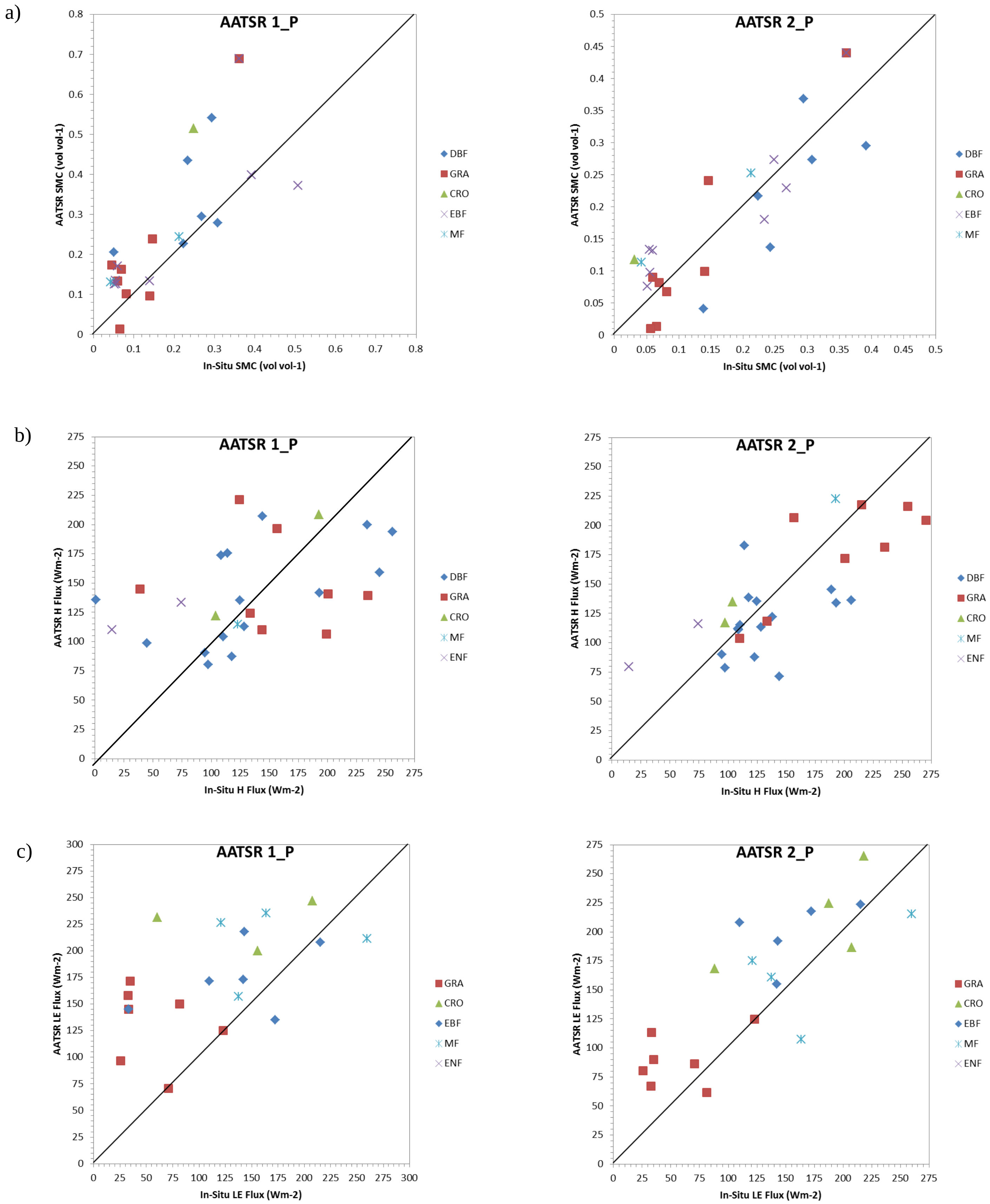

Figure 4: *Scatterplots displaying the agreement between the half-hourly AATSR estimated values and CarboEurope in-situ measurements of; a) soil moisture content* (cm^3 cm^{-3})*, b) instantaneous sensible heat (H) flux (Wm^{-2}), and c) instantaneous latent heat (LE) flux (Wm^{-2}). The plots on the left hand side display the results stratified by land cover type obtained by the inversion method based on the non-atmospherically corrected product (AATSR 1P). The plots on the right hand side display the results stratified by land cover type obtained by the inversion method based on the atmospherically corrected product (AATSR 2P) (DBF – Deciduous Broadleaf Forest, GRA – Grassland, CRO – Cropland, MF – Mixed Forest, ENF – Evergreen Needle-leaf Forest).*

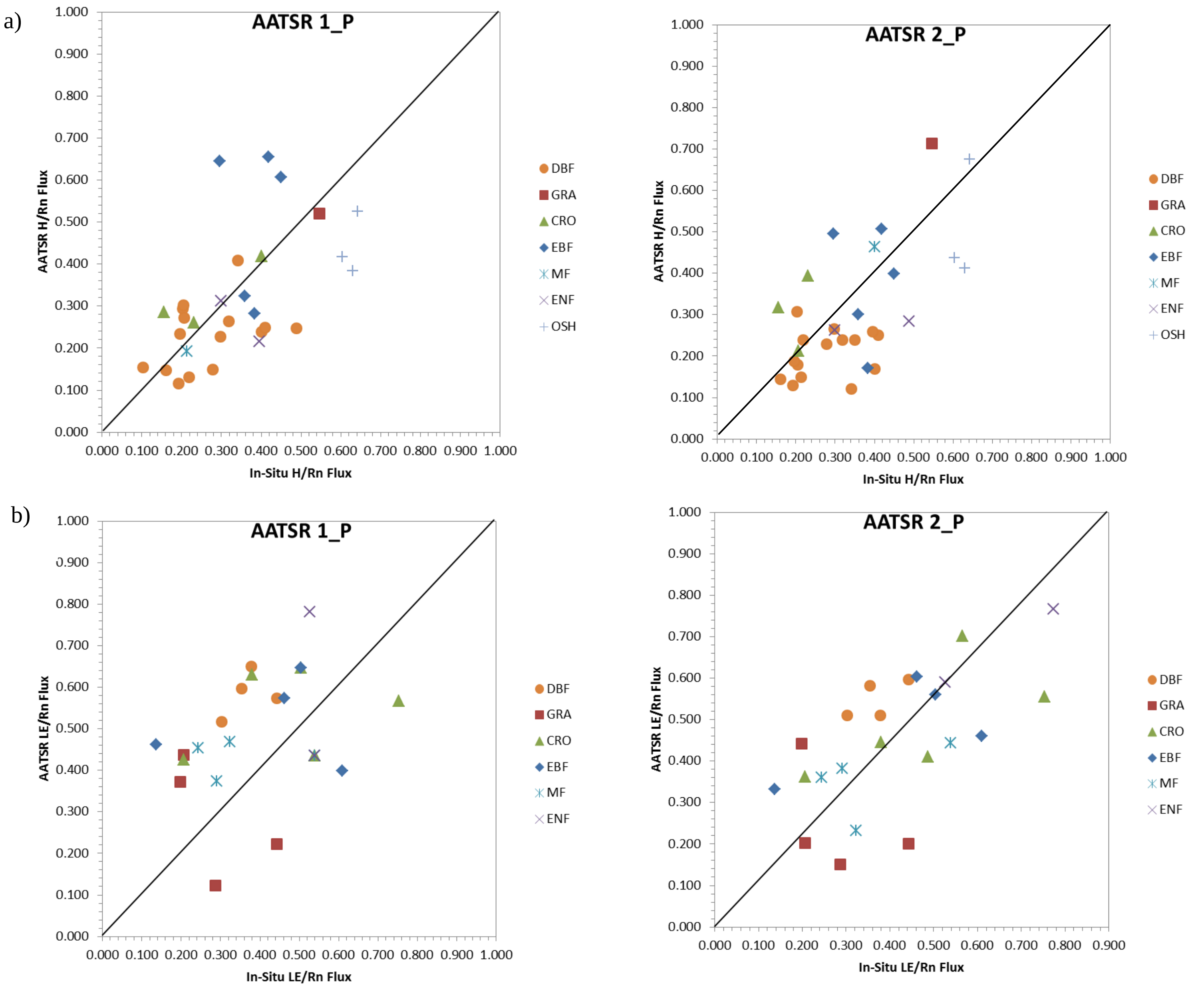

Figure 5: *Scatterplots displaying the agreement between the half-hourly AATSR estimated values and CarboEurope in-situ measurements of; a) daytime averaged sensible heat (H/Rn) flux, and b) daytime averaged latent heat (LE/Rn) flux. The plots on the left hand side display the results stratified by land cover obtained by the inversion method based on the non-atmospherically corrected product (AATSR 1P). The plots on the right hand side display the results stratified by land cover type obtained by the inversion method implementation based on the atmospherically corrected product (AATSR 2P) (DBF – Deciduous Broadleaf Forest, GRA – Grassland, CRO – Cropland, MF – Mixed Forest, ENF – Evergreen Needle-leaf Forest).*

Table 1: *Location and characteristics of the CarboEurope flux tower sites used in our study*

Site Name	Site Abbreviation	Geographic Coordiantes	Country	PFT Land Cover	Elevation	Climate
Aguamarga	ES-Agu	36.8347/-2.2511	SPAIN	Open Shrubland - OSH	199m	Arid Steppe cold
Amoladeras	ES-Amo	36.9405/-2.0329	SPAIN	Open Shrubland - OSH	58m	Arid Steppe cold
Collelongo-Selva Piana	IT-Col	41.8493/13.588	ITALY	Deciduous Broadleaf Forest - DBF	1560m	Warm temperate fully humid with hot summer
Renon/Ritten (Bolzano)	IT-Ren	46.5878/11.435	ITALY	Evergreen Needleleaf Forest - ENF	1730m	Snow fully humid cool summer
Lecceto	IT-Lec	43.3046/11.271	ITALY	Evergreen Needleleaf Forest - ENF	314m	Warm temperate fully humid with hot summer
Nonantola	IT-Non	44.6898/11.089	ITALY	Mixed Forest - MF	20m	Warm temperate fully humid with hot summer
Malga Arpaco	IT-Mal	46.1167/11.703	ITALY	Grassland - GRA	1730m	Polar tundra
Bonis	IT-Bon	39.4778/16.535	ITALY	Evergreen Needleleaf Forest - ENF	1170m	Warm temperate with dry, hot summer
Negrisia	IT-Neg	45.7476/12.447	ITALY	Cropland - CRO	9m	Warm temperate fully humid with warm summer
Castellaro	IT-Cas	45.0700/8.7175	ITALY	Cropland - CRO	84m	Warm temperate fully humid with hot summer
Espirra	PT-Esp	38.6394/-8.6018	PORTUGAL	Evergreen Broadleaf Forest - EBF	95m	Warm temperate with dry, hot summer
Mitra IV Tojal	PT-Mi2	38.4765/-8.0246	PORTUGAL	Grassland - GRA	190m	Warm temperate with dry, hot summer

Table 2: *Definition of the statistical performance measures used to assess the agreement between the "triangle"-derived estimates, and the in-situ observations. Subscripts i = 1, … N denote the individual observations at N distinct locations, P denotes the predicted values, and O denotes the "observed" values. In this study the observed values are obtained from the selected CarboEurope sites. The horizontal bar in Scatter / MSD ratio equation denotes the mean value evaluated over the N sites. The summation in the correlation coefficient is over all the sites.*

Name	Description	Mathematical Definition
Bias / MBE	Bias (accuracy) or Mean Bias Error	$bias = MBE = \frac{1}{N}\sum_{i=1}^{N}(P_i - O_i)$
Scatter / MSD	Scatter (precision) or Mean Standard Deviation	$scatter = \sqrt{\frac{1}{(N-1)}\sum_{i=1}^{N}(P_i - O_i - \overline{(P_i - O_i)})^2}$
RMSD	Root Mean Square Difference	$RMSD = \sqrt{bias^2 + scatter^2}$
MAD	Mean Absolute Difference	$MAD = N^{-1}\sum_{i=1}^{N}\lvert P_i - O_i \rvert$
R	Linear Correlation Coefficient	$R = \frac{n\sum xy - (\sum x)(\sum y)}{\sqrt{n(\sum x^2) - (\sum x)^2}\sqrt{n(\sum y^2) - (\sum y)^2}}$